Supporting Information for "Modulation Doping of GaAs/AlGaAs Core–Shell Nanowires With Effective Defect Passivation and High Electron Mobility"

Jessica L. Boland,[†] Sonia Conesa-Boj,[‡] Patrick Parkinson,[†] Gözde Tütüncüoglu,[‡] Federico Matteini,[‡] Daniel Rüffer,[‡] Alberto Casadei,[‡] Francesca Amaduzzi,[‡] Fauzia Jabeen,[¶] Christopher L. Davies,[†] Hannah. J. Joyce,[§] Laura M. Herz,[†] Anna Fontcuberta i Morral,[‡] and Michael B. Johnston[*,†]

Department of Physics, University of Oxford, Oxford, OX1 3PU, United Kingdom, Laboratory of Semiconductor Materials, École Polytechnique Fédérale de Lausanne (EPFL), CH-1015 Lausanne, Switzerland, Laboratory for Quantum Mechanics, École Polytechnique Fédérale de Lausanne (EPFL), CH-1015 Lausanne, Switzerland, and University of Cambridge, Centre for Advanced Photonics and Electronics, 9 JJ Thomson Avenue, Cambridge CB3 0FA, United Kingdom

E-mail: m.Johnston1@physics.ox.ac.uk

---

[*] To whom correspondence should be addressed

[†] Clarendon Laboratory

[‡] Laboratory of Semiconductor Materials

[¶] Laboratory for Quantum Mechanics

[§] Department of Engineering

Experimental Details

Nanowire Growth

For both samples, the nanowires were grown on a native oxide covered (111) Si substrate by the catalyst-free gallium assisted method in a DCA P600 solid source MBE system. For the modulation doped sample, growth of the GaAs core has been done with a growth rate of 0.5 Å/s, V/III of 20 and a substrate temperature of 640°C. Prior to the growth of the AlGaAs shell, gallium flux has been cut for 20 minutes in order to consume the droplet, following which the growth is switched from axial to radial growth conditions by decreasing the substrate temperature to 495°C and increasing the V/III to 80 by increasing the arsenic flux to 1.2×10^{-5} torr. The modulation doped sample is grown under a rotation of 15 rpm to increase the uniformity whereas undoped core/shell sample is grown with 7 rpm. For the undoped sample, the GaAs core was grown at a rate of 0.3 Å/s, V/III of 40 and a substrate temperature of 640°C. The AlGaAs shell was grown by increasing the arsenic flux to 1.3×10^{-5} torr to give a V/III of 100, and lowering the substrate temperature to 480°C. Thus the growth conditions for both samples were very similar, showing that they are appropriate for comparison.

Transmission Electron Microscopy

High-angle annular dark-field scanning transmission electron microscopy (HAADF STEM) cross-section images were performed using a FEI Tecnai OSIRIS microscope operated at 200 kV at the Centre Interdisciplinaire de Microscopie Électronique (CIME) at EPFL Lausanne. The same microscope was used to characterize the crystalline structure and the defect density along the nanowire axis. For such measurements, the nanowires were mechanically transferred to a holey carbon grid. A reconstruction of a representative nanowire along the axial direction is shown in Figure S1 for the undoped sample. The crystalline structure turns out to be Zinc-Blende and the main type of defects observed are twin defects. From the difference in contrast in the respective bright field TEM images, the density of defects in the various regions can be determined. The lower end of the NW is the one that corresponds to the beginning of the growth, where the density of twin defects is small. As we move along the nanowire length the density of twins increases, up to a maximum of about 80 twins/micrometer at the opposite end. The distribution of defects is similar both for the doped and the reference samples, as expected since the distribution of defects is determined by the GaAs core, which has been grown with similar growth parameters in both samples. Figure S2 shows TEM images for a modulation doped nanowire, clearly showing the twin defects in the zinc–blende crystalline structure that are distributed along the axial direction of the nanowire.

Cross-section Sample Preparation

Cross-sections of the nanowires from both the doped and the reference samples were prepared by microtomy, as illustrated in Figure S3. The first step was to isolate part of a substrate on which the vertical nanowires had been grown (1). This was achieved using a small cubic block of polydimethylsiloxane (PDMS) in which a hole though the centre was used as a mask. The PDMS block was placed on the wafer, and the hole used to define the nanowires to be studied. Epoxy resin was then poured into the hole in the PDMS block and the resin was then stabilized by exposure to UV light (2). After this, the PDMS block was separated from the wafer by pressing on one side (3) and the epoxy resin cylinder containing the nanowires was removed from the PDMS (4). The resin cylinder was larger than the grid on which the slices were to be deposited. Therefore, a razor blade was used to remove the surface of the resin cylinder around the region of interest, forming a truncated pyramid (5). Next, the nanowire containing epoxy was mounted on a ultramicrotome system and sliced with a diamond knife into slices with thickness of 40 nm (6). The resulting epoxy slices were then collected in a deionised water bath behind the knife and picked up with a droplet of water using a perfect loop and then transferred to a TEM grid (7). At this point, nanowire

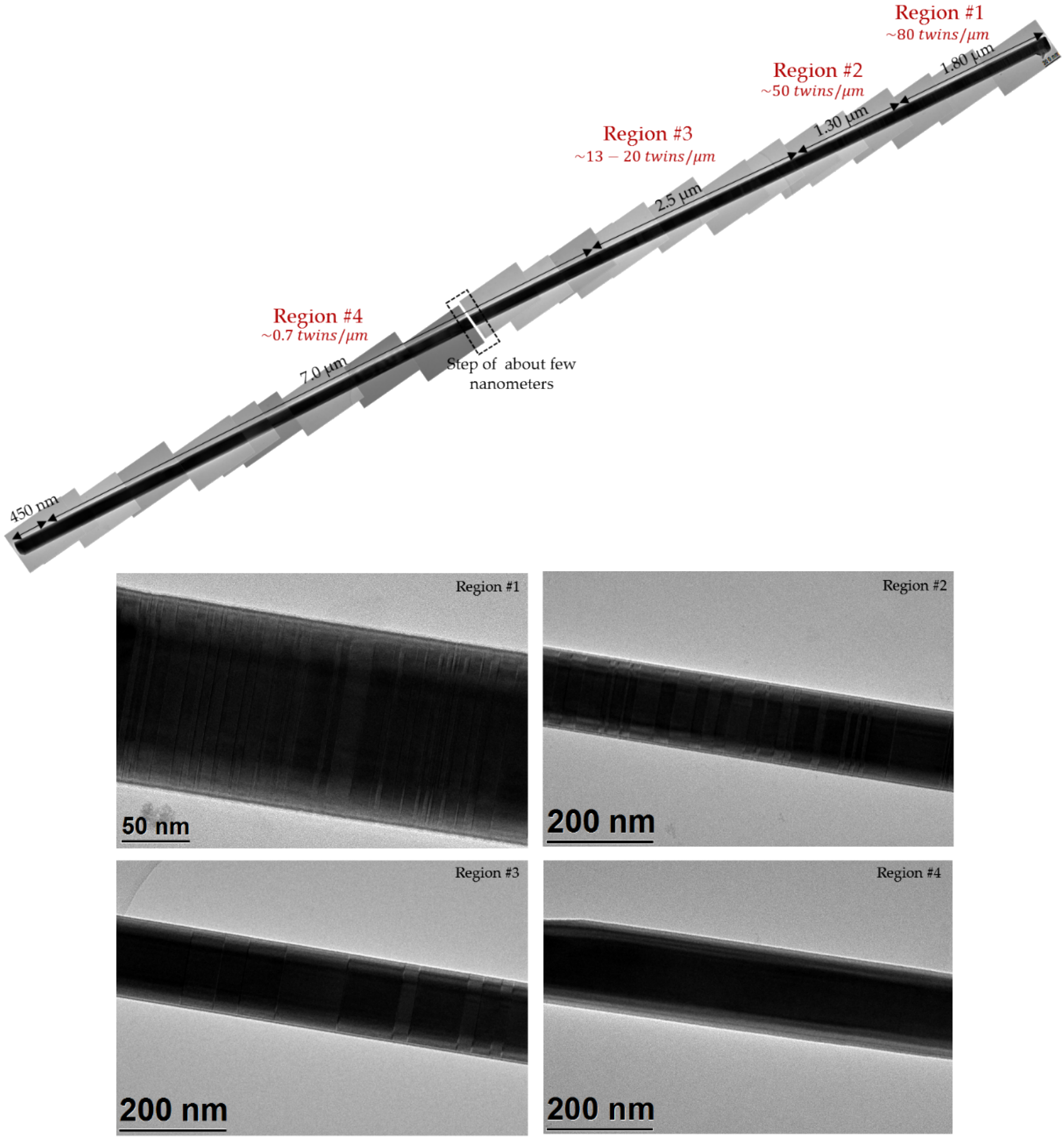

Figure S1: Upper image, reconstruction of a representative nanowire of the undoped sample, indicating the various regions with different densities of twin defects. Lower images bright field TEM images from the various regions shown in the nanowire reconstruction.

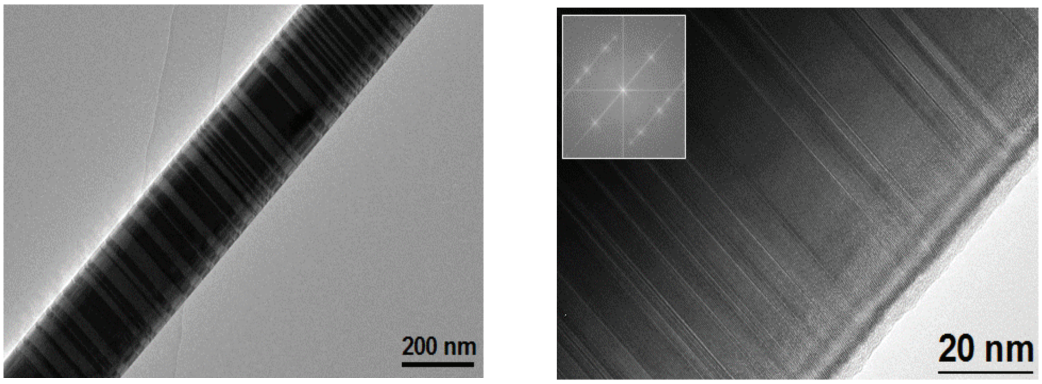

Figure S2: Low magnification TEM image of a modulation doped nanowire exhibiting the presence of stripes with different contrast along its length (left). These stripes correspond to twin defects in the zinc–blende crystalline phase, as can be seen from the corresponding HRTEM image (right).

cross-sections were ready to be analysed in the electron microscope (8).

Terahertz Time-Domain Spectroscopy

An amplified Ti:Sapphire laser with an average power of $4\,\mathrm{W}$ was used to generate $35\,\mathrm{fs}$ pulses centred at $800\,\mathrm{nm}$ at a repetition rate of $5\,\mathrm{kHz}$. Each pulse was separated into three different paths: $590\,\mu\mathrm{J}$/pulse as an optical pump to photoexcite the sample; $200\,\mu\mathrm{J}$/pulse to generate the THz probe via optical rectification in a 2mm GaP crystal; and $1.6\,\mu\mathrm{J}$/pulse as a gate beam for electro-optical detection of the transmitted THz pulse via a $200\,\mu\mathrm{m}$ GaP crystal. In order to obtain a range of sample photoexcitation fluences between $5\,\mu\mathrm{J\,cm^{-2}}$to $26\,\mu\mathrm{J\,cm^{-2}}$, the optical pump beam was attenuated by neutral density filters. At the sample, the full width half maximum (FWHM) for the optical pump beam is $10\,\mathrm{mm}$ and for the THz probe is $1\,\mathrm{mm}$, so that the THz probe measures an area of homogenous photoexcited carrier density. The THz electric field, E, was measured using a balanced photodiode circuit and

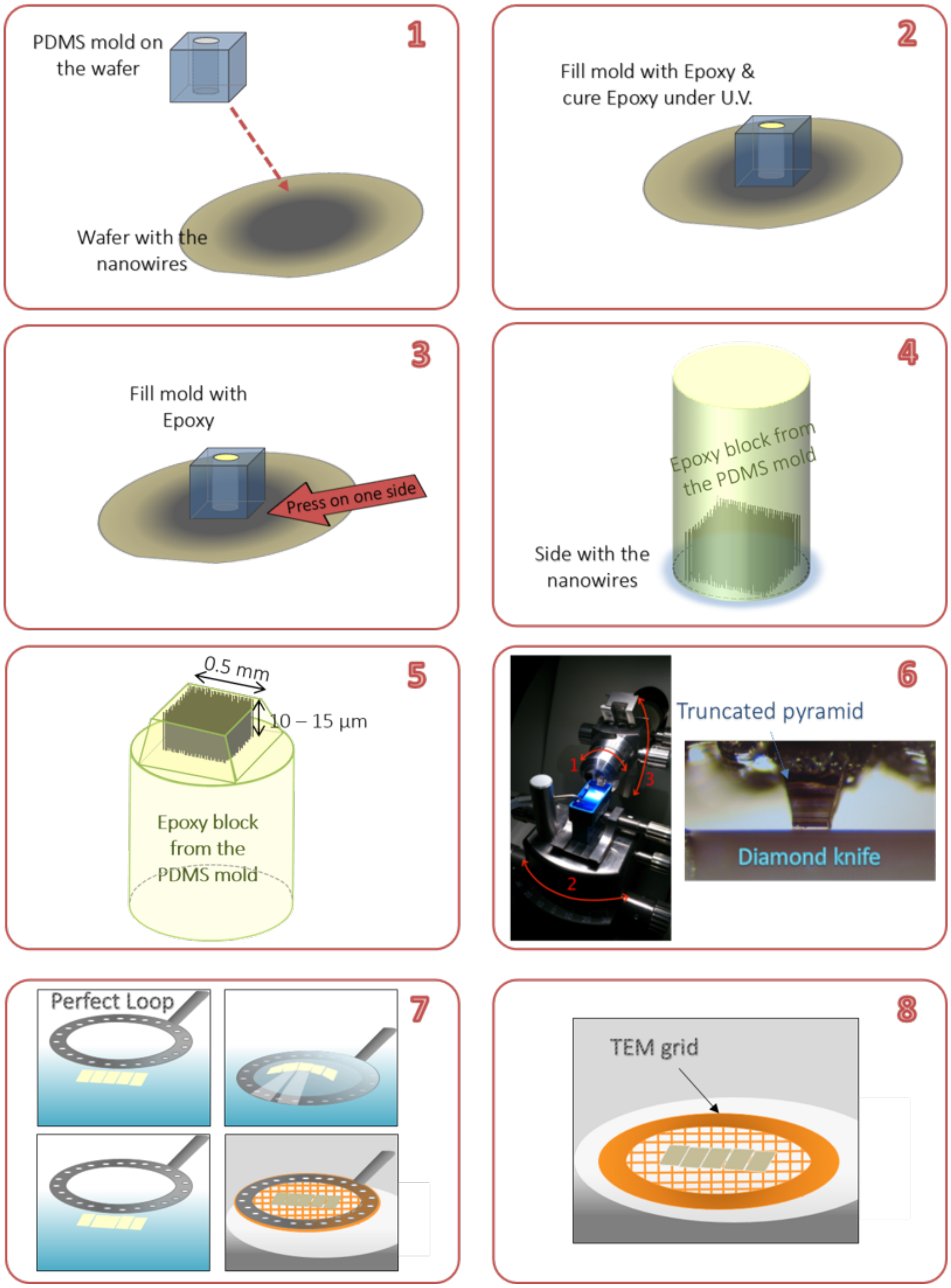

Figure S3: Schematic illustration of the procedure used to prepare the nanowire cross-section, see text for description of the various steps.

a lock-in amplifier referenced to a chopper at 2.5 kHz in the THz generation beam. The optical pump-induced change in the THz electric field, ΔE was measured using a second lock-in amplifier referenced to a chopper at 125 Hz in the optical pump beam. By varying the time delays between all three beams, a 2D map of the THz spectral response as a function of time after photoexcitation can then be measured. All measurements were taken at room temperature with the THz beam under vacuum to avoid any absorption of THz radiation by atmospheric water vapour.

Time-Resolved Micro-Photoluminescence

Time-resolved micro photoluminescence (μ-PL) was performed using a homebuilt optical system equipped with time-correlated single photon counting. An ultrafast pulsed Ti:Sapphire laser (100 fs pulse duration) tuned to 800 nm was used to photoexcite the sample with a fluence of approximately 0.2 μJ/cm^2. Both the excitation, and the emitted PL were imaged using a 40x magnification objective lens providing a spatial resolution of around 100 μm. The emitted light was spectrally filtered (using a 880 nm ±70 nm bandpass filter) to remove the residual scattered excitation pulse, and was focused onto the entrance slit of a 160 mm spectrograph equipped with a 300 lines/mm grating. The dispersed photoluminescence was collected by directing it onto a single-photon silicon avalanche photodiode for time-resolved measurements. A time-resolution of approximately 40 ps was achieved with a maximum range of 12 ns set by the repetition rate of the laser oscillator (see Figure S6).

Simulations of Energy Band Levels for the Modulation Doped Sample

Figure S4 shows simulations of the energy band levels for the modulation doped sample with and without photoexcitation. The simulations are carried out by using the nextnano software, which consists of a Schrödinger-Poisson solver for modelling semiconductor nanowire

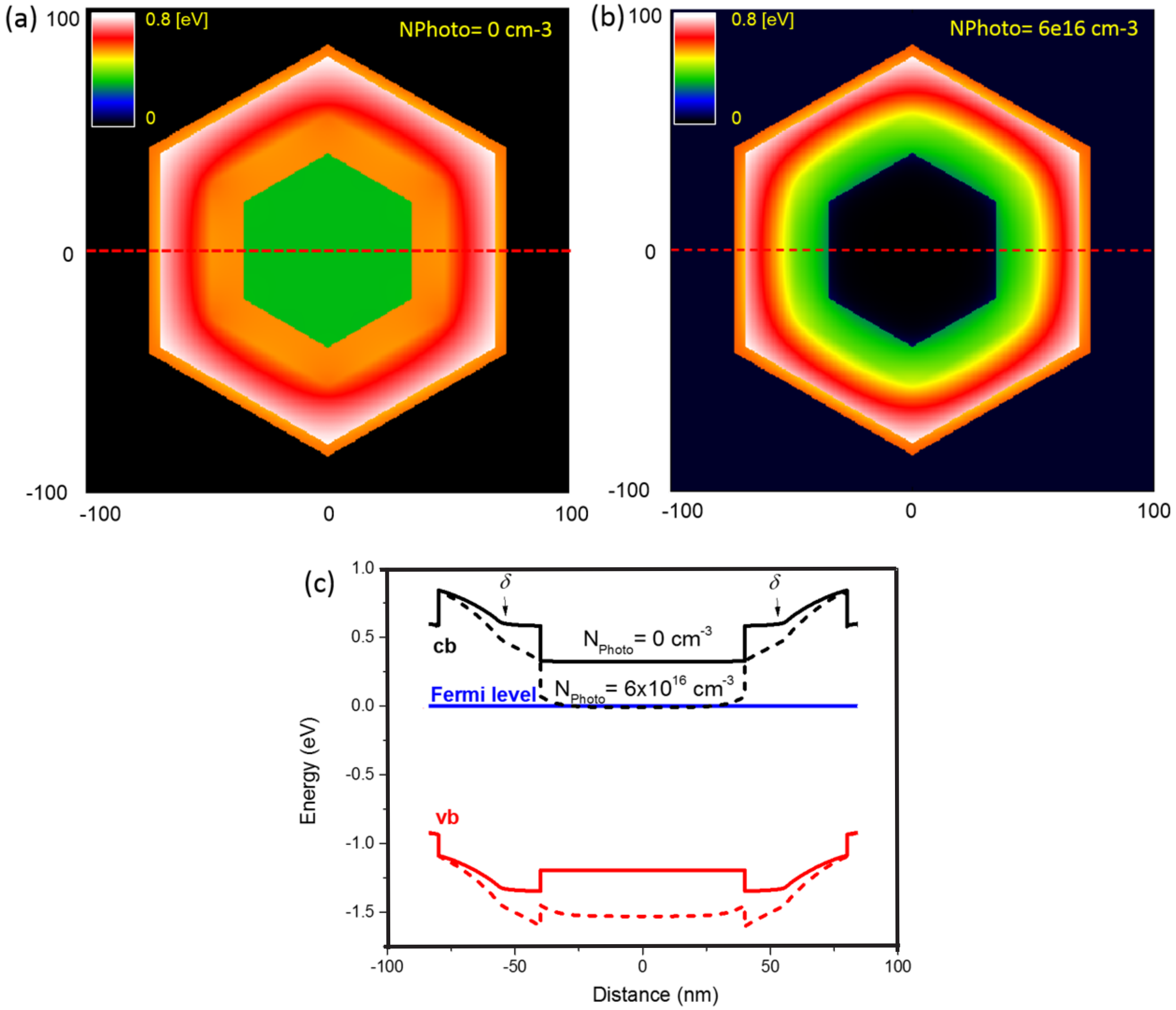

Figure S4: Nextnano simulations of the conduction band level for a cross-section of the modulation doped nanowire a) without photoexcitation and b) with photoexcitation contributing to a photoexcited electron density of $6 \times 10^{16} cm{-}3$. c) Energy band diagram for the modulation doped nanowire as a function of distance from the core with and without photoexcitation.

structures.[1] Material parameters can be entered to model any nanostucture and both the undoped and doped samples have been modelled. In Figure S4, it can be clearly seen that the delta doped layer alters the energy level of the conduction band, with the level increasing up until the capping layer. When photoexcited, the conduction band level in the core of the nanowire sits at the Fermi level and the conduction band level within the shell lowers, allowing for carrier transport in the nanowire.

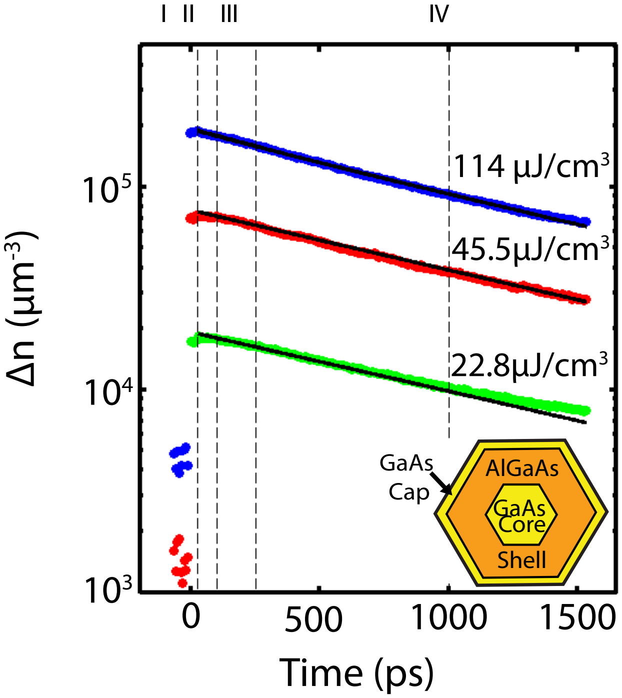

Figure S5: Pump-induced change of carrier concentration against pump–probe delay for the undoped GaAs nanowires at fluences of 22.8, 45.5, 114 μJ cm^{-2}.

Fluence Dependence for Undoped Reference Sample

Figure S5 shows the decay of the carrier density with time after photoexcitation for the undoped GaAs nanowires at excitation fluences of 22.8, 45.5, 114 μJ cm^{-2}. The decay traces clearly show a a monoexponential decay with a shorter lifetime in comparison to modulation doped GaAs nanowires. The data also shows that there is no bimolecular recombination, as the decay traces have the same decay rate for each fluence. By fitting the carrier rate equation to the data, the decay constant for this behaviour, k_1, was determined to be $6.67 \pm 0.26 \times 10^9\,\mathrm{s}^{-1}$, giving a photoinjected charge carrier recombination lifetime of $1.5 \pm 0.38\,\mathrm{ns}$.

Fluence Dependence of Photoconductivity Spectra for Modulation Doped Sample and Undoped Reference

Figure S6 presents photoconductivity spectra of GaAs/algaas core–shell nanowires obtained at a range of different photoexcitation fluences. The left–hand column shows displays spectra of the n–type modulation doped sample, while those in the right–hand column correspond to the undoped reference sample. Spectra were taken 100ps after photoexcitation with $1.5eV\,(800\,nm)$ at fluences of 0.46, 1.14, 4.55, 11.4, 22.8, 45.5, 114 and 225 $\mu\mathrm{J\,cm}^{-2}$. All spectra show a Lorentzian response, with the resonant frequencies (marked by the arrows in Figure S6) shifting to higher frequency with increasing excitation fluence. The resonant frequency increasing with increasing carrier density is a key attribute of localised surface plasmon (LSP) modes. The resonant frequency is also clearly shifted to higher frequency for the modulation doped sample (left column) compared with the undoped reference (right column) for each excitation fluence. This is related to the additional donated electrons in the doped nanowires, as described by Equation 4 in the main manuscript. The results shown in Figure S6 are summarised in Figure 4a of the main manuscript, where each spectrum corresponds to one point in the Figure 4a.

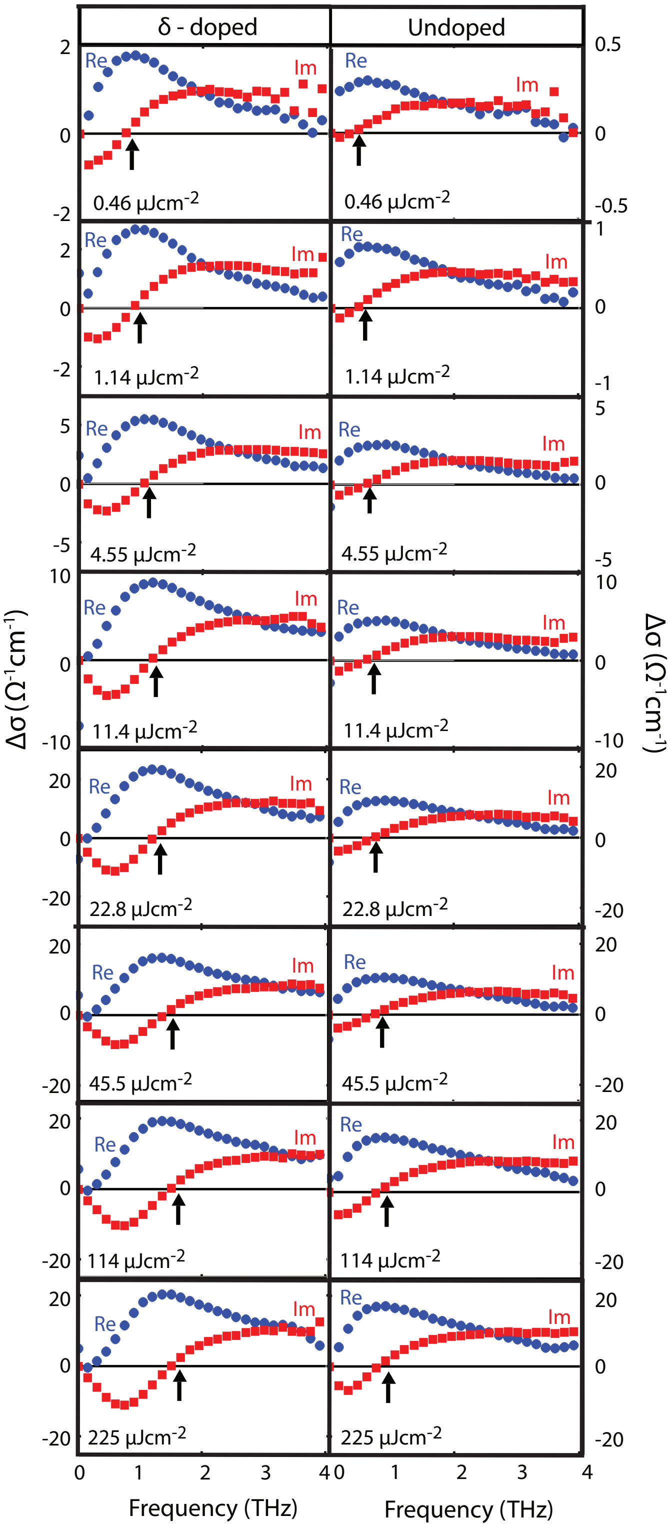

Figure S6: Time–resolved conductivity of photoexcited carriers for the undoped reference sample taken 100ps after photoexcitation at the following fluences 0.46, 1.14, 4.55, 11.4, 22.8, 45.5, 114 and 225 μJ cm^{-2}

Photoluminescence Lifetimes

Figure S7 shows the PL intensity against time after photoexcitation for both the modulation doped and undoped nanowires at an excitation fluences of approximately 0.2 μJ cm^{-2}at 800nm. A dark response function was also taken to give a reference for the background noise in the system. This dark response function was then subtracted from the data to remove the baseline. An instrument response function (IRF) was also taken, giving a time resolution of the system of 40ps. As the PL lifetimes of both samples are over 1ns, it is assumed that this response function has minimal effect on the data. The data were then fitted with an exponential function, as seen in Figure S4 to give PL lifetimes of 1.11 ± 0.17 ns and 2.39 ± 0.05 ns. for the undoped and modulation doped nanowires respectively.

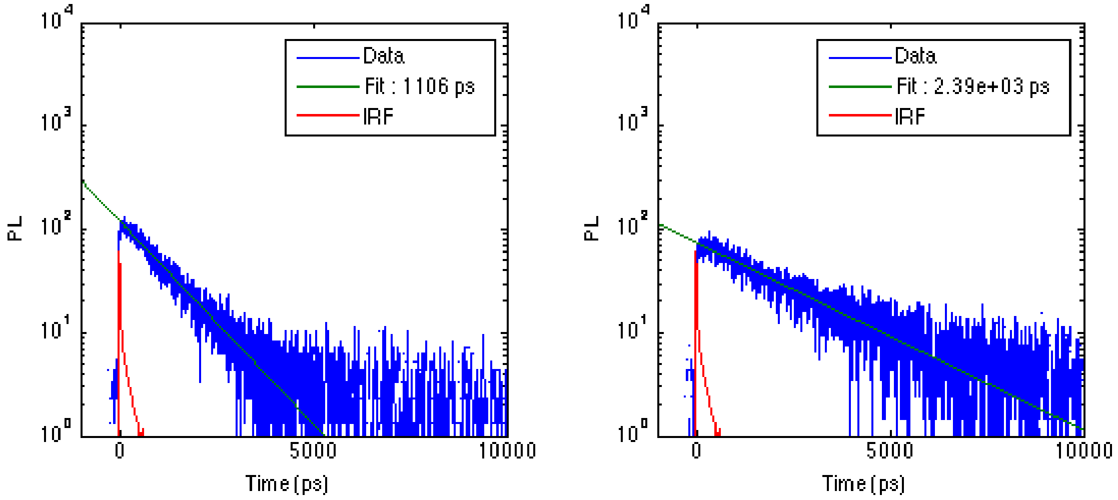

Figure S7: Normalised photoluminescence against time in picoseconds for a) undoped and b) modulation doped GaAs nanowires photoexcited at a wavelength of 800nm with a fluence of 0.2 μJ cm^{-2}. The IRF (red) and exponential fit (green) are shown on top of the data.

Data Analysis of THz Transmission Data

Conversion of THz Transmission to Photoconductivity

The photoconductivity, $\Delta\sigma$, is extracted from the OPTP measurements of $\frac{\Delta E}{E}$. The nanowires are considered to be embedded within a surrounding layer of thickness, d, which is the average diameter of the nanowire; and to have an effective areal fill factor obtained from optical microscope images.[2] The transmitted terahertz fields with and without the optical pump are described as follows:

$$E_{\mathrm{on}} = f_{\mathrm{w}} E_{\mathrm{w}*} + (1 - f_{\mathrm{w}})\, E_{\mathrm{v}} \tag{1}$$

$$E_{\mathrm{off}} = f_{\mathrm{w}} E_{\mathrm{w}} + (1 - f_{\mathrm{w}})\, E_{\mathrm{v}}. \tag{2}$$

where E_{w} and E_{v} are the terahertz transmitted electric fields through the nanowires and surrounding vaccum respectively, with * denoting a photoexcited state. The pump beam does not change the complex refractive index of the vacuum, so the electric fields E_{v}, E_{w} and $E_{\mathrm{w}*}$ can be written as:

$$E_{\mathrm{v}} = e^{in_{\mathrm{v}}\omega d/c} E_{\mathrm{i}} \tag{3}$$

$$E_{\mathrm{w}} = t_{\mathrm{vw}} t_{\mathrm{wv}} e^{in_{\mathrm{w}}\omega d/c} FP_{\mathrm{vwv}} E_{\mathrm{i}} \tag{4}$$

$$E_{\mathrm{w}*} = t_{\mathrm{vw}*} t_{\mathrm{w}*\mathrm{v}} e^{in_{\mathrm{w}*}\omega d/c} FP_{\mathrm{vw}*\mathrm{v}} E_{\mathrm{i}}. \tag{5}$$

where t_{ij} are the Fresnel transmission coefficients, FP_{ijk} the Fabry-Pérot terms, c is the speed of light and $n_{\mathrm{w}*}$, n_{w} the refractive indices for the nanowires with and without photoexcitation respectively. By combining Equations 1 and 2, the ratio of terahertz fields for the nanowires with and without photoexcitation is given in terms of the OPTP measurement of

$\frac{\Delta E}{E}$:

$$\frac{E_{\mathrm{w}*}}{E_{\mathrm{w}}} = \frac{\Delta E}{E}\left[1 + \left(\frac{1}{f_{\mathrm{w}}} - 1\right)\frac{E_{\mathrm{v}}}{E_{\mathrm{w}}}\right] + 1. \tag{6}$$

where $\Delta E = E_{\mathrm{on}} - E_{\mathrm{off}}$, the photoinduced change in transmission and $E = E_{\mathrm{off}}$, the THz transmission in the absence of photoexcitation. At THz frequencies, the thin film limit can be applied, as $\frac{n\omega\delta}{c} >> 1$, so the approximation $\frac{E_{\mathrm{v}}}{E_{\mathrm{w}}} = 1$ can be made. By using this approximation, a parameter A can be defined:

$$A = \frac{E_{\mathrm{w}}}{E_{\mathrm{w}*}} = \frac{1}{\frac{1}{f_{\mathrm{w}}}\frac{\Delta E}{E} + 1}. \tag{7}$$

By substituting in the appropriate FP_{ijk} and t_{ij} into Equation 3 and 4 and applying the thin film limit, the following equation is obtained:

$$\frac{E_{\mathrm{w}*}}{E_{\mathrm{w}}} = \frac{2 - \frac{i\omega d}{c}\left(1 + n_{\mathrm{w}}^2\right)}{2 - \frac{i\omega\ d}{c}\left(1 + n_{\mathrm{w}*}^2\right)}. \tag{8}$$

Substituting in the general relation $n^2 = \epsilon$ to the above equation:

$$\epsilon_{\mathrm{w}*} = \left[-\frac{E_{\mathrm{w}}}{E_{\mathrm{w}*}}\left(2\frac{c}{i\omega d} - (1 + \epsilon_{\mathrm{w}})\right) + 2\frac{c}{i\omega d} - 1\right]. \tag{9}$$

where $\epsilon_{\mathrm{w}*}$ and ϵw are the dielectric constants of the nanowires with and without photoexcitation respectively. The photoinduced conductivity, $\Delta\sigma$ is then given by:

$$\epsilon_{\mathrm{w}*} = \epsilon_{\mathrm{w}} + \frac{i\Delta\sigma}{\omega\epsilon_0}. \tag{10}$$

where ϵ_0 is the permittivity of free space. Substituting Equation 9 into Equation 10, the photoinduced conductivity can be extracted:

$$\Delta\sigma = \epsilon_0 \left(A - 1\right) \left[\frac{2c}{d} - i\omega \left(1 + \epsilon_{\mathrm{w}}\right)\right]. \tag{11}$$

Thus, using Equations 7 and 11, the photoinduced conductivity can be extracted from OPTP measurements using $\epsilon_{\mathrm{w}} = 12.95$ for bulk GaAs and values of f_{w} and d taken from optical electron microscope measurements.

Calculating the Photoexcited Carrier Density

The photoexcited carrier density, n_{p} for a sample of thickness d is given by:

$$n_{\mathrm{p}} = \frac{I}{Ed}\left(1 - e^{-d/\alpha}\right). \tag{12}$$

where I is the photoexcitation fluence, E is the photon energy and α is the absorption depth at the excitation wavelength. The absorption depth, $\frac{1}{\alpha}$ for GaAs is approximately 1μm for photons with energy $1.5eV\;(800nm)^3$. This absorption depth is significantly larger than the nanowire diameter studied, so the nanowires fall within the thin film limit. Therefore, for a given photoexcitation intensity, the photoexcited carrier density is approximately constant for the nanowire diameter.

Fitting Process for Carrier Decay Traces and Conductivity Spectra

The charge carrier recombination dynamics for nanowires depend on excitation fluence and are described by the following carrier rate equation:[4]

$$\frac{dn\left(t\right)}{dt} = -k_1 n - k_2 n^2 - k_3 n^3. \tag{13}$$

where k_1 is the decay constant describing the rate of mono-molecular processes, such as trap-assisted recombination, k_2 is the bimolecular recombination constant and k_3 is the rate for Auger recombination. This carrier rate equation was globally fitted to the experimental data, by fixing the decay constants for each different excitation fluence for each sample.

The fitting process is a nonlinear least-square fit that requires the following optimisation:

$$min_x||f\left(x\right)||_2^2 = min_x\left(f_1\left(x\right)^2 + f_2\left(x\right)^2 + ...f_n\left(x\right)^2\right). \tag{14}$$

The fitting process starts from an initial point and minimises the sum of the squares of the function described above. A lower bound of zero was placed on all the fitting parameters to make sure that they remain positive and therefore physical.

The same fitting process was used to globally fit a Lorentzian conductivity response to the photoconductivity spectra with the doping density set as a global parameter for the undoped and doped sample respectively. The uncertainty for the doping density parameter calculated using the chi-squared non-linear regress was found to be 5.4 % for the undoped sample and 8.2 % for the doped sample.

Empirical Low-Field Mobility Model for Fitting to Spectral Data

The model used to fit to the extracted mobilities from the spectral data is a Caughey-Thomas-like, empirical, mobility model, with temperature-dependent parameters.[5] The mobility model suggests that if the low-field mobility of a particular material is known as a function of T and N, the mobility of any other material can be obtained by scaling the same formula with a constant factor. Thus, the mobility is given by:

$$\mu = \mu_{\mathrm{min}} + \frac{\mu_{\mathrm{max}} - \mu_{\mathrm{min}}}{1 + \left(\frac{n_{\mathrm{ref}}}{n}\right)^{\gamma}}. \tag{15}$$

where μ_{min} is the minimum electron mobility and μ_{max} the maximum electron mobility for the system, n_{ref} is the carrier concentration at which the mobility reduces to half its maximum value at low doping and γ a scaling factor related to the system. At high doping concentrations, the mobility saturates at μ_{min}, which is temperature-independent; and at very low doping concentrations, the mobility saturates at μ_{max}, which is the lattice-limited mobility and reduces with increasing temperature.

References

(1) Birner, S.; Zibold, T.; Andlauer, T.; Kubis, T.; Sabathil, M.; Trellakis, A.; Vogl, P. *IEEE Trans. Electron Devices* **2007**, *54*, 2137–2142.

(2) Joyce, H. J.; Wong-Leung, J.; Yong, C.; Docherty, C. J.; Paiman, S.; Gao, Q.; Tan, H. H.; Jagadish, C.; Lloyd-Hughes, J.; Herz, L. M.; Johnston, M. B. *Nano Lett.* **2012**, *12*, 5325–5330.

(3) Casey, H. C.; Sell, D. D.; Wecht, K. W. *J. Appl. Phys.* **1975**, *46*, 250–257.

(4) Aspnes, D. E. *Surf. Sci.* **1983**, *132*, 406–421.

(5) Sotoodeh, M.; Khalid, A. H.; Rezazadeh, A. A. *J. Appl. Phys.* **2000**, *87*, 2890–2900.